Imperfect Fabry-Perot resonators

Klaassen, T.

CHAPTER 6

Connection between wave and ray approach of cavity aberrations

We connect the wave and ray description of spherical aberration in a cavity. The link we use is Fermat's principle in a frequency-degenerate cavity. In the ray picture, we consider periodically closed orbits beyond the paraxial limit and calculate the reduction in cavity length that is needed to compensate for the additional (nonparaxial) fourth-order terms. In the wave picture, we derive and discuss explicit expressions for the nonparaxial contribution to the Gouy phase. This Chapter combines and compares results from Chapter 4 and 5.

6.1 Introduction

The first analysis of frequency-degenerate Fabry-Perot cavity was based on a ray description. This analysis involved a calculation of the total path length $L_{\mathrm{tot}}(\rho)$ of a closed orbit as a function of transverse amplitude ρ of the ray. Pioneering work was done by Hercher [19], Bradley and Mitchell [45], Arnaud [47], and Ramsay and Degnan [46]. We have generalized this analysis from the confocal resonator, $K/N = 1/2$, to an arbitrary K/N frequency-degeneracy, in Chapter 4.

Only recently, Visser *et al.* used a different approach based on wave optics. In their calculation, they benefited from the analogy between the paraxial wave-equation and the Schrödinger equation, using a quantum mechanical operator description for the evolution of the field profile [62]. Spherical aberration was included via a fourth-order term related to the mirror height profile. In this Chapter, we will extend this wave approach by including another term that was previously overlooked. In many cases this extra term, which is also fourth-order and related to the transverse momentum of the ray, dominates.

The challenge to connect the above ray and wave description has not yet been accomplished. We will do so in this Chapter. The key to success is the application of Fermat's principle in a frequency-degenerate cavity. For rays, this principle states that the realized closed orbit is the one that extremizes the total path length, making $dL_{\mathrm{tot}}(\rho)/d\rho = 0$. To preserve the closed orbit beyond paraxiality, the cavity length should be reduced for increased transverse displacement. For waves, a similar requirement of "complete recovery after N round-trips" imposes frequency-degeneracy of the cavity eigenmodes. More precisely, it requires that the Gouy phase of the contributing modes differs by multiples of $2\pi/N$. We will derive an expression for the nonparaxial contribution to the Gouy phase and show that higher-order modes (again) require a reduction in cavity length to maintain the phase relation of the superposition after N round-trips. The comparison between the ray and wave result, finally provides for the necessary link between both pictures.

In Section 6.2, we review the ray description of Chapter 4 and use it in order to calculate the mentioned reduction in cavity length. In Section 6.3, we extend the standard wave description beyond the paraxial regime. We briefly review the wave description introduced in [62], and extend it by including the nonparaxial contribution of the transverse momentum of the ray. In Section 6.4, we compare the results from the ray and wave description by relating the transverse ray displacement to the mode number. We end with a concluding discussion in Section 6.5.

6.2 Ray description of spherical aberration

The general idea of this Section is as follows. We assume a closed orbit inside a symmetric two-mirror resonator with spherical aberration operated close to a $1/N$ frequency-degenerate cavity length. We stretch the closed orbit without changing the position of the hit points on the mirrors. Obviously, the angles of reflection on the mirror have to change to preserve the closed orbit. The only physical trajectories, where the angle of incidence on the mirrors equals the angle of reflection, are found by Fermat's principal.

First, we review the ray description of the total path length of a closed orbit as presented

in Chapter 4. The central concept in this ray description is the average path length of a closed orbit, where the nth hit point at one mirror is given by $x_n = \rho \sin(n\theta_0 + \phi_0)$ [49] with ρ the transverse amplitude, θ_0 the round-trip Gouy phase, and ϕ_0 an additional phase that determines the type of orbit (with extreme cases: the V-shaped and the bow-tie orbit). This total path length is (see Eq. 4.1 in Chapter 4)

$$\frac{1}{2N} L_{\mathrm{tot}}(\rho) = L - B(L - L_{\mathrm{res}}) \frac{\rho^2}{R^2} - A \frac{\rho^4}{R^3} \,, \tag{6.1}$$

where L is the on-axis cavity length and $L_{\mathrm{res}} = R[1 - \cos(\theta_0/2)]$ is the paraxial resonance length (at $\rho \approx 0$) for exact $1/N$-degeneracy. For $(N \geq 3)$ the spherical aberration coefficient A and the detuning coefficient B are (see Eqs. 4.2 and 4.3 in Chapter 4)

$$A = \frac{1 + \cos(\theta_0/2)}{32\,[1 - \cos(\theta_0/2)]} = \frac{2R - L_{\mathrm{res}}}{32 L_{\mathrm{res}}} \quad \text{and} \tag{6.2}$$

$$B = \frac{1}{2}\left[\frac{1}{1 - \cos(\theta_0/2)}\right] = \frac{R}{2L_{\mathrm{res}}} \,. \tag{6.3}$$

Equation 6.1 describes the average length of a mathematically closed orbit, but this orbit does not necessarily fulfill the physical requirements of reflection angles. Special orbits are the ones that also fulfill the latter requirement, which is most compactly formulated via Fermat's principle $dL_{\mathrm{tot}}(\rho)/d\rho = 0$. Taking the derivative of Eq. 6.1 and setting $dL_{\mathrm{tot}}(\rho)/d\rho = 0$ we obtain

$$\Delta L \equiv L - L_{\mathrm{res}} = -\frac{2A}{B}\frac{\rho^2}{R} = -\frac{z_0^2}{2RL}\frac{\rho^2}{R} \,, \tag{6.4}$$

where $z_0 = \frac{1}{2} k_0 w_0^2 = k_0 \gamma_0^2 = \frac{1}{2}\sqrt{2RL - L^2}$ is the Rayleigh-range, k_0 is the wavevector, and w_0 and γ_0 are two different measures for the fundamental beam waist. As both coefficients A and B in Eq. 6.4 are positive for stable resonators ($L < 2R$), off-axis (nonparaxial) rays require a cavity length reduction to satisfy Fermat's principle.

For completeness, we note that the above expressions for A and B do not hold for $N = 2$. For $N = 2$, the two extreme orbits, the V-shaped and a bow-tie orbit, have different coefficients A and B. This can easily be understood as the maximum transverse deviations x_n are ρ and $\rho/\sqrt{2}$ for the V-shaped ($\phi_0 = 0$) and the bow-tie ($\phi_0 = \theta_0/4$) orbit, respectively. Furthermore, the V-shaped orbit does not show spherical aberration, *i.e.*, $A = 0$, as the incident ray at the off-axis hit points is normal to the mirror surface. Hercher's result for the bow-tie orbit is

$$\frac{1}{2N} L_{\mathrm{tot}}(x_n) = L - (L - L_{\mathrm{res}}) \frac{x_n^2}{R^2} - \frac{x_n^4}{4R^3} \,, \tag{6.5}$$

where $x_n = \rho/\sqrt{2}$ is the maximum transverse deviation and ρ being the transverse amplitude.

For $N = 2$ there is also an exact solution of the form [63]

$$L_{\mathrm{tot}}(\alpha) = 4R\left[2 - \frac{1}{\cos(\alpha/2)}\right] \,, \tag{6.6}$$

where α is the angle of the diagonal ray in the bow-tie. The cavity length reduction, predicted by this exact solution is $\Delta L = -R\alpha^2/8$. As $\alpha \approx 2x_n/R$ in a confocal resonator, this result is consistent with the restriction $dL_{\mathrm{tot}}(x_n)/dx_n = 0$, which yields $\Delta L = -x_n^2/(2R)$ when applied to Eq. 6.5.

6.3 Wave description of spherical aberration

The paraxial description of a symmetric two-mirror resonator of length L with mirror curvatures R (see Fig. 6.1) is centered around the concept of the round-trip Gouy phase

$$\theta_0(L) = 2\arccos(1 - L/R) \, . \tag{6.7}$$

Changes in the cavity length will modify this (paraxial) Gouy phase via the derivative

$$d\theta_0(L)/dL = \frac{2}{\sqrt{L(2R-L)}} = \frac{1}{z_0} \, . \tag{6.8}$$

In a 1D (planar) description of the cavity field, the phase delay of the m-th order Hermite-Gauss mode as compared to a plane wave is

$$\Psi_m = (m + \tfrac{1}{2})\theta_0 \, . \tag{6.9}$$

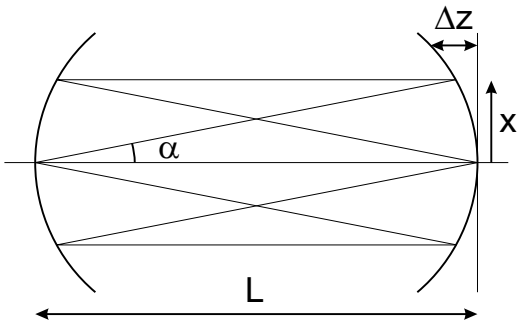

Figure 6.1: *Sketch of a symmetric two-mirror cavity of length L comprising two mirrors with radius of curvature R. The mirror curvature is characterized by the height profile Δz. The closed orbit is threefold frequency-degenerate ($N = 3$). The slope of the rays is characterized by the angle α.*

For larger beam displacements, *i.e.*, higher-order modes, an additional nonparaxial term contributes to the Gouy phase. Roughly speaking, the phase delay of m-th order Hermite-Gauss mode as compared to a plane wave can be separated in a linear and nonlinear contribution of the form (see Chapter 5)

$$\Psi_m \equiv \Psi_{\text{lin.}} + \Psi_{\text{nonlin.}} \approx am + bm^2 \, , \tag{6.10}$$

where $a = \theta_0(L)$ is the paraxial Gouy phase.

The nonparaxial term in Eq. 6.10 is a measure for the aberrations. It shows that a change in cavity length is needed to maintain frequency-degeneracy for higher-order modes also in the nonparaxial wave description. When the derivative $(\Psi_{m+1} - \Psi_{m-1})/2 = a + 2bm$ is fixed to a multiple of $2\pi/N$, degeneracy is fulfilled. The derivative $a + 2bm$ remains constant for

a higher-order mode m by lowering a (b is a higher-order correction). Using $a = \theta_0(L) = \theta_0(L_0) + [d\theta_0(L)/dL]\Delta L$, we thus obtain

$$\Delta L = \frac{-2bm}{d\theta_0(L)/dL} = -2bmz_0 \, . \tag{6.11}$$

We find again that the cavity length has to be reduced to maintain frequency-degeneracy within a set of higher-order modes. In the next Subsections, we will derive an explicit expression for $b > 0$ in terms of R and L, to further quantify this length reduction.

6.3.1 Effect of mirror shape (x^4-term)

Visser *et al.* [62] have given a wave description of two-mirror resonators, based on the mirror profile $\Delta z(x)$ shown in Fig. 6.1. Their description is essentially based on the expansion of the mirror profile $\Delta z(x)$ beyond the paraxial quadratic terms as

$$\Delta z = R - \sqrt{R^2 - x^2} \approx \frac{x^2}{2R} + \frac{x^4}{8R^3} \, , \tag{6.12}$$

where the fourth-order term acts as small perturbation. This term, describing the spherical aberration of the mirror, acts as the following perturbation on the potential in a Schrödinger-type equation

$$V_{\rm eff}(x) = \frac{1}{16kR}(1-g^2)\frac{x^4}{\gamma^4} \, , \tag{6.13}$$

where $g \equiv 1 - L/R$ (see Eq. (37) of Visser *et al.* [62]). For a fixed cavity length L, the perturbation slightly shifts the frequency of a mode with mode number m.

The (in-plane) 1D-version of Eq. (50) in Visser *et al.* [62] predicts a round-trip phase delay of

$$\Psi_m = \Psi_{\rm lin.} + \Psi_{\rm nonlin.} \approx 2\arccos\left(1 - \frac{L}{R}\right)(m + \tfrac{1}{2}) + \frac{L}{2kR(2R-L)}\left(\tfrac{3}{2}m^2 + \tfrac{3}{2}m + \tfrac{3}{4}\right) \, , \tag{6.14}$$

where the first terms combine Eqs. 6.7 and 6.9, and the second term quantifies the nonlinear contribution to the round-trip phase delay via

$$\Psi_{\rm nonlin.} \approx b_x m^2 = \frac{3L}{4kR\,(2R-L)}m^2 \, , \tag{6.15}$$

assuming $m^2 \gg (m + \frac{1}{2})$. Note that we have included a subscript x to b_x to distinguish this mirror-based contribution from the momentum-based contribution b_p discussed in the next Subsection.

6.3.2 Effect of slope in rays (p^4-term)

The above description was based on a Taylor-expansion of the mirror height profile only. A more complete description is obtained if we also account for the higher-order terms in the Taylor-expansion of the transverse momentum

$$k_z = k_0\cos(\alpha) = \sqrt{k_0^2 - p^2} \approx k_0 - \left(\frac{p^2}{2k_0} + \frac{p^4}{8k_0^3}\right) , \tag{6.16}$$

where $p = k_0 \sin(\alpha)$ is the transverse momentum of the ray at angle α. The quadratic term in the expansion corresponds to the paraxial wavevector. The fourth-order term gives rise to an additional nonparaxial contribution. The perturbation on the potential associated with this contribution is [64]

$$W_{\text{eff}}(p) = \frac{1}{4kL}\frac{1-g}{1+g}\gamma^4 p^4 \,. \tag{6.17}$$

Straightforward calculus shows that the b_p coefficient derived for this momentum-based term is larger than the b_x coefficient derived above by a factor $2R/L$, making

$$b = b_x + b_p = \frac{3L}{4kR(2R-L)}\left(1+\frac{2R}{L}\right) \,. \tag{6.18}$$

The existence of a p^4-term on top of a x^4-term is also touched upon in Section 8.5, where an analysis based on the effective index method gives exactly the same ratio ($2R/L$) between these two terms. The importance of the fourth-order term in the Taylor-expansion of the momentum has been discussed in several other papers that go beyond the paraxial regime [65, 66].

6.4 Comparison of wave and ray description

In the two previous Sections, we have used both the ray and wave description to calculate the reduction in cavity length that is needed to retain frequency-degeneracy beyond the paraxial regime, *i.e.*, for large transverse amplitudes ρ, *c.q.*, modes with large mode number m. In the ray description, we obtained Eq. 6.4, which reads

$$\Delta L = -\frac{2A}{B}\frac{\rho^2}{R} = -\frac{z_0^2}{2RL}\frac{\rho^2}{R} \,. \tag{6.19}$$

In the wave description, we obtained Eq. 6.11, which reads

$$\Delta L = -2bmz_0 = \frac{-3L(2R+L)}{8kRz_0}m \,. \tag{6.20}$$

In order to compare these calculated length reductions ΔL, we need to relate the squared displacement amplitude ρ^2 to the mode number m. This relation is $\rho^2 = 2m\gamma^2$ [12], where the waist at the mirror is $\gamma^2 = \gamma_0^2[1+(z/z_0)^2] = \gamma_0^2[LR/(2z_0^2)]$. Substitution of this relation in Eq. 6.19 yields

$$\Delta L = -\frac{z_0^2}{2RL}\frac{\rho^2}{R} = -\frac{z_0}{2kR}m \,. \tag{6.21}$$

A quantitative comparison of Eqs. 6.20 and 6.21 shows that the required length reductions are different for the ray and wave description. For a general cavity length

$$\frac{\Delta L_{\text{ray}}}{\Delta L_{\text{wave}}} = \frac{2R-L}{3(2R+L)} \,. \tag{6.22}$$

Only in the short cavity limit $L \ll R$, Eq. 6.20 becomes comparable to Eq. 6.21. In this limit, the ray result Eq. 6.20 yields

$$\Delta L = \frac{-3z_0}{2kR} m \,. \tag{6.23}$$

In the short cavity limit, the ray and wave description of spherical aberration are thus identical except for a prefactor.

6.5 Concluding discussion

To shed light on the difference between the ray and the wave descriptions of cavity aberrations, we have tried to determine their validity experimentally. Unfortunately, this attempt failed for two reasons. First of all, the relation between the measured phase delay θ_m and mode number m was not strictly linear, as was predicted by theory and demonstrated experimentally for a folded three-mirror resonator (see Ch. 5). Secondly, and more important, the relation depended strongly on the alignment of the cavity and the injection of the beam. Apparently, the mirror surface is nonspherical and contributes additional aberrations on top of the ones calculated in this Chapter.

In conclusion, we have presented an extension of the wave description of spherical aberration, introducing a term that was previously overlooked. Furthermore, we have tried to reconcile results from the ray model presented in Chapter 4 and wave models presented in Chapter 5 and ref. [62]. We could link both models using the cavity length reduction needed to preserve frequency-degeneracy beyond paraxiality. This attempt was successful only in the short cavity limit. This somewhat surprising result is not yet fully understood.